



Photonic quantum Hall effect and multiplexed light sources of large orbital angular momenta

Babak Bahari¹, Liyi Hsu¹,², Si Hui Pan¹, Daryl Preece¹, Abdoulaye Ndao², Abdelkrim El Amili¹, Yeshaiahu Fainman¹ and Boubacar Kanté (10,12,3,4 ⋈

The quantum Hall effect involves electrons confined to a two-dimensional plane subject to a perpendicular magnetic field, but it also has a photonic analogue¹⁻⁶. Using heterostructures based on structured semiconductors on a magnetic substrate, we introduce compact and integrated coherent light sources of large orbital angular momenta⁷ based on the photonic quantum Hall effect¹⁻⁶. The photonic quantum Hall effect enables the direct and integrated generation of coherent orbital angular momenta beams of large quantum numbers from light travelling in leaky circular orbits at the interface between two topologically dissimilar photonic structures. Our work gives direct access to the infinite number of orbital angular momenta basis elements and will thus enable multiplexed quantum light sources for communication and imaging applications.

In 1879, Edwin Hall discovered the classical Hall effect, a consequence of the motion of charged particles in a magnetic field⁸. The quantum Hall effect was discovered almost exactly a century later in 1980 by Klaus von Klitzing by applying a transverse magnetic field to a two-dimensional electron gas confined in semiconductor heterojunctions9. Since then, the quantum Hall effect has continuously intrigued due to its non-trivial transport properties and exotic topological phases10. The quantum Hall effect was extended to photonic systems to implement robust quantum Hall topological waveguides, cavities, thermal photon spin and light sources¹⁻⁶. Topological effects have been successfully investigated in photonics using various platforms that implement synthetic gauge fields in different regimes¹¹⁻¹⁴, Floquet topological insulators^{15,16}, bianisotropic metacrystals¹⁷ and the valley Hall effect^{18,19}. Using heterostructures based on structured semiconductors on a magnetic substrate, we propose compact and integrated coherent light sources of large orbital angular momenta (OAM) based on the photonic quantum Hall effect. Orbital angular momentum is a fundamental degree of freedom of photons characterized by the quantum number ℓ (ref. 7). The unbounded nature of the quantum number is a unique attribute that enables high-capacity communication, quantum cryptography or increased resolution in classical and quantum imaging²⁰. The proposed sources give direct access to the infinite number of OAM basis elements and can thus enable applications in spintronics, microscopy and metrology. Previous methods to directly generate OAM from lasers are either more suited for small quantum numbers or non-integrated when large quantum numbers are considered^{21–24}. Compact and integrated sources capable of directly multiplexing and generating arbitrarily large ℓ have remained elusive. We demonstrate quantum numbers as large as 276. The generated beams are

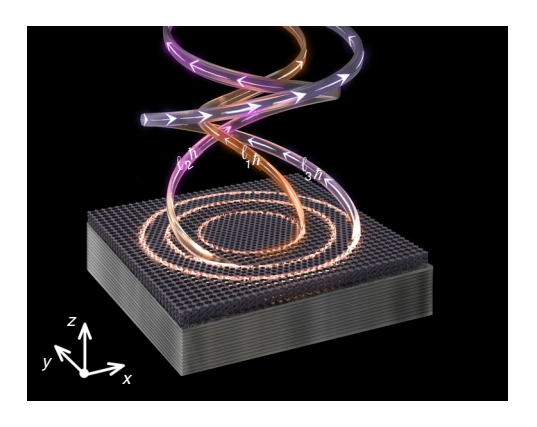


Fig. 1 | Photonic QH rings and integrated OAM of large quantum numbers. Schematic of the integrated leaky QH ring lasers (lasers 1, 2 and 3) emitting OAM beams with quantum numbers ℓ_1 , ℓ_2 and ℓ_3 . \hbar is the reduced Planck constant. Each QH ring laser has a length $m\lambda_{eff}$, where m is an integer representing the azimuthal order of the one-way whispering gallery mode and $\lambda_{\rm eff}$ is the guided wavelength in the mode. The propagation phase offsets at different points of the travelling wave around a leaky ring result in far-field interference and the formation of OAM beams with quantum numbers equal to the azimuthal resonant order of the ring ($\ell = m$). The quantum number of the emitted OAM beam can thus be made large, a unique attribute of the proposed platform. Integrated concentric QH rings are formed by alternating circular boundaries between topologically dissimilar photonic bandgap materials. The photonic crystal with a square lattice (PhC1) has a non-trivial bandgap. The photonic crystal with a triangular lattice (PhC2) has a trivial bandgap. The photonic crystals are patterned in InGaAsP multiple quantum wells. The non-trivial topology is obtained by bonding InGaAsP on a flat yttrium iron garnet substrate under a static magnetic field normal to the surface of the photonic crystals, $\mathbf{B} = B_0 \mathbf{e}_1$.

experimentally characterized using self-interference and the coherence of beams is confirmed using a Hanbury Brown–Twiss interferometer. Furthermore, we demonstrate the natural integration of three coherent OAM sources sharing the same aperture, a principle that can be used to integrate multiple light sources. Our experimental results constitute coherent topological light sources that can generate topological light on demand and enable novel quantum light sources for communication and imaging.

The platform shown in Fig. 1 is made of circular boundaries between topologically dissimilar photonic crystals forming two-dimensional cavities referred to as photonic quantum Hall rings

¹Department of Electrical and Computer Engineering, University of California San Diego, La Jolla, CA, USA. ²Department of Electrical Engineering and Computer Sciences, University of California, Berkeley, CA, USA. ³Department of Mechanical Engineering, University of California Berkeley, Berkeley, CA, USA. ⁴Materials Sciences Division, Lawrence Berkeley National Laboratory, Berkeley, CA, USA. [™]e-mail: bkante@berkeley.edu

NATURE PHYSICS LETTERS

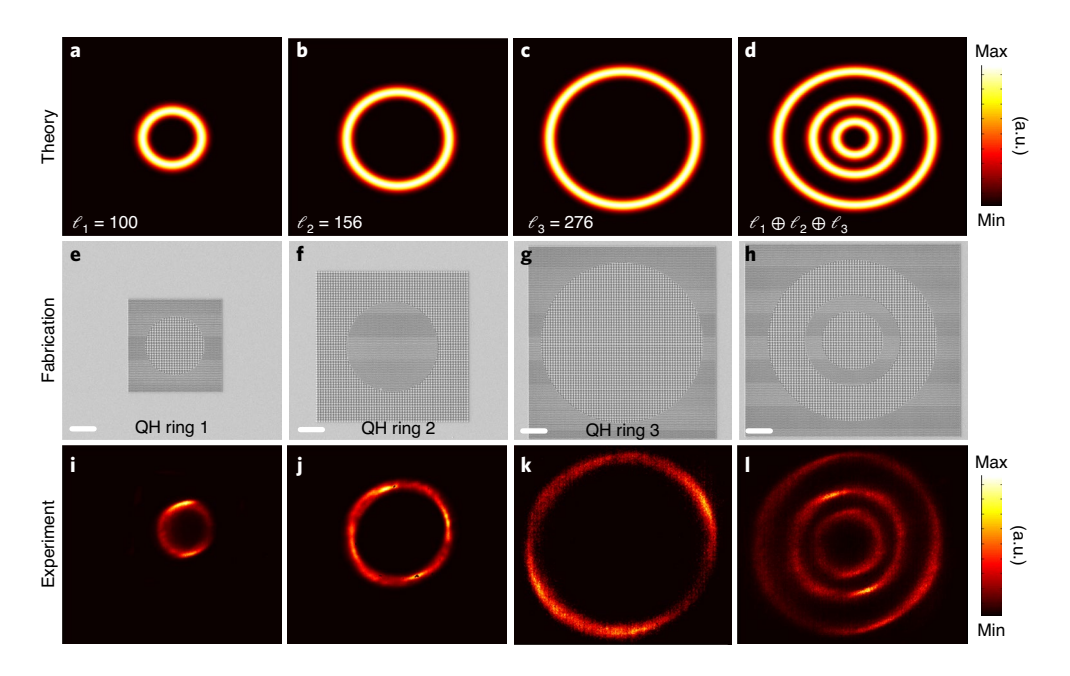


Fig. 2 | Simulation, fabrication and luminescence of photonic QH rings. a-d, Theoretical prediction of the far field for QH ring 1 (**a**), ring 2 (**b**), ring 3 (**c**) and their superposition (**d**). The one-way edge state is modelled by its dominating in-plane field components (Supplementary Information). **e-h**, Top-view scanning electron micrographs of the QH rings formed by the non-trivial (PhC1) and trivial (PhC2) photonic crystals. **e-g**, The circular boundary encloses PhC1 in QH ring 1 (**e**), PhC2 in QH ring 2 (**f**) and PhC1 again in QH ring 3 (**g**), resulting in edge states propagating clockwise in rings 1 and 3 and anticlockwise in ring 2. The quantum numbers of the fabricated rings are $|\ell_1|$ = 100, $|\ell_2|$ = 156 and $|\ell_3|$ = 276. The structures are fabricated on InGaAsP by electron-beam lithography followed by dry etching and then bonded on an yttrium iron garnet substrate. **h**, Integrated QH rings corresponding to the planar superposition of QH ring 1, ring 2 and ring 3. Scale bars are 10 μm, and the unit cells of PhC1 and PhC2 have a periodicity of p = 1,084 nm and p/3, respectively. **i-l**, Luminescence, under B_0 = 100 Oe and uniform pumping with a pump wavelength of 1,064 nm, from QH ring 1 (**i**), ring 2 (**j**), ring 3 (**k**) and their superposition (**l**). These images are taken from the surface of each device.

(QH rings). The dissimilar topologies of the photonic structures inside and outside the OH ring ensures the existence of one-way circulating edge states at their boundary. While our original topological laser was intended to generate non-reciprocal light on a chip via a waveguide3, here, for an edge state above the light cone, QH rings made of 2.5D photonic structures in the XY plane are leaky-wave vertical emitters (topological antennas) designed to deliver light out of the chip. They thus radiate in the third dimension (Z direction) out of the plane, as shown in Fig. 1. The propagation phase offsets at different points of the travelling wave around the leaky ring result in the formation of OAM beams in the far field where the quantum number is equal to the azimuthal resonant order of the ring. The quantum number of the OAM beam can, therefore, be made large with the radii of the rings. By alternating concentric circular boundaries between the two topologically dissimilar photonic crystals, multiple orthogonal OAM beams of alternating chirality can be integrated in a planar manner using a single aperture. This is shown in Fig. 1, where three QH rings—patterned in the same aperture—emit three concentric OAM beams. The structure shown in Fig. 1 contains two photonic crystals. Photonic crystal one (PhC1) is formed by a four-armed star-shaped unit cell and has a non-trivial bandgap (Supplementary Information). Photonic crystal two (PhC2) has a triangular lattice with a cylindrical air-hole unit cell and a trivial bandgap (Supplementary Information). The topologically non-trivial photonic crystal is obtained by bonding the structured InGaAsP multiple quantum wells on a flat and unstructured yttrium iron garnet substrate, as shown in Fig. 1. The yttrium iron garnet substrate is used to break the time-reversal symmetry in the system under a static external magnetic field perpendicular to the substrate that opens the non-trivial gap of PhC1. The size of the bandgap can be further increased by using a bismuth iron garnet substrate or structuring the magnetic material to increase its

overlap with the optical mode. However, this would make the fabrication process more complex and also increase optical losses. Circular boundaries between PhC1 and PhC2 are leaky-wave QH rings (QH ring 1, QH ring 2 and QH ring 3), as shown in Fig. 1.

Figure 2 shows the theoretical prediction of the far-field emission from QH ring 1 (Fig. 2a), QH ring 2 (Fig. 2b), QH ring 3 (Fig. 2c) and the superposition of these three rings (Fig. 2d). The one-way edge state is modelled by its dominating in-plane field components (Supplementary Information). The three rings are designed for the quantum numbers $\ell_1 = 100$, $\ell_2 = 156$ and $\ell_3 = 276$, and they are naturally orthogonal states. It is worth noting that there is a minimum number of unit cells needed to create a bandgap. The finite size of the nanostructures thus signifies that ring n and ring n+1cannot be infinitely close. Since a minimum number of unit cells are needed to create a bandgap in periodic structures^{25,26}, the smallest OAM mode depends on the photonic crystal used. In our case, if the trivial photonic crystal (with periodicity $p_{trivial} = 361.3 \text{ nm}$) is placed between two non-trivial photonic crystals, the distance between the two rings would be $\Delta r = 3p_{\text{trivial}} = 1,083.9 \text{ nm}$ (number of trivial cells needed for an edge state). Thus, based on the formula $r/\lambda_{\text{eff}} = \ell/2\pi$, the topological charge difference between rings n and n+1 would be $\Delta \ell = 9$. For the same reason, by using the trivial photonic crystal at the centre, the minimum topological charge that can be generated by our platform would be $\ell = 5$.

The structures are fabricated by electron-beam lithography, etching and bonding (Supplementary Information). Figure 2e-h shows the top-view scanning electron micrographs of the QH rings, showing the quality of nanofabrication. The circular boundary encloses PhC1 in QH ring 1 (Fig. 2e), PhC2 in QH ring 2 (Fig. 2f) and PhC1 again in QH ring 3 (Fig. 2g); further, the three concentric rings are clearly visible, as shown in Fig. 2h. The integrated QH rings (Fig. 2h), realized using one-step lithography, consist of the planar

LETTERS NATURE PHYSICS

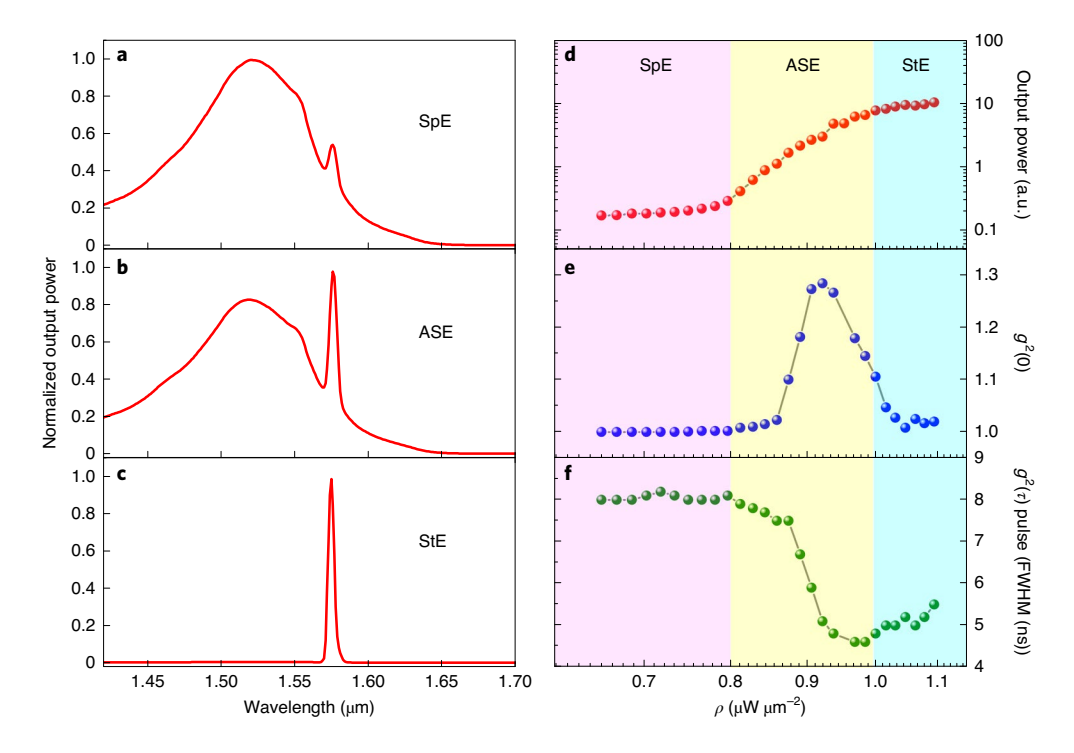


Fig. 3 | Lasing characteristics and photon statistics of photonic QH rings. a-c, Photoluminescence spectrum of optically pumped QH ring 2 in the presence of an external magnetic field B_0 =100 Oe in the SpE (a), ASE (b) and StE (c) regimes. The surface of the laser is uniformly pumped with a pump laser at 1,064 nm. The amplification and selection of a single mode are observed when the pump power is increased. d, Output power as a function of the pump power (light-light curve). The threshold pump power density (average power) is about 1 μ W μ m⁻². e,f, Second-order intensity correlation at zero-delay $g^2(0)$ (e) and its FWHM (f). Clearly, the photon bunching peak (in the ASE regime of $g^2(0)$) is suppressed in the StE regime and the FWHM of $g^2(\tau)$ shrinks, reaches a minimum in the ASE regime and broadens in the StE regime, unambiguously demonstrating the lasing action of the QH ring.

integration of ring 1, ring 2 and ring 3 in a single aperture. The cavities are characterized by optically pumping the entire surface of the crystals in the presence of a static external magnetic field $\mathbf{B} = +B_0\mathbf{e}_z$ $(B_0$ is the magnitude of the magnetic field and \mathbf{e}_z is the unit vector perpendicular to the photonic crystals plane) that saturates the yttrium iron garnet material. The micro-photoluminescence setup pumps the sample from the top with a pulsed laser ($\lambda_{pump} = 1,064 \text{ nm}$ and T = 6 ns pulse at a repetition rate of 290 kHz) using an objective lens. The emission from the devices, as shown in Fig. 2, is collected using the same objective lens and directed to a monochromator for spectrum analysis or to an infrared camera for imaging. The images shown in Fig. 2i-l are collected when the surface of the lasers coincides with the focal plane of the objective lens that forms an image of the aperture (surface of the QH rings) at infinity on the infrared camera. The rings thus undergo the same magnification, and the ratios of the distances between the bright rings are the same as the ratios of their physical separation. Far-field intensity patterns of the beams generated by QH rings 1, 2, 3 and their superposition exhibit light localization in the QH rings.

To further characterize the emission from the devices, Fig. 3a–c shows the photoluminescence spectrum of optically pumped QH ring 2 in the presence of B_0 in three different regimes. The amplification and selection of a single mode at wavelength $\lambda = 1,575\,\mathrm{nm}$ can be observed with increasing pump power. Similar results were observed for other QH rings. Figure 3d shows the log-scale output power as a function of the pump power density (light–light curve) and shows a characteristic lasing behaviour. To further investigate the coherent character and lasing characteristic of the QH ring, we measured the second-order intensity correlation function of its emission, $g^2(\tau) = \frac{I(t)I(t+\tau)}{I(t)^2}$, using a Hanbury Brown–Twiss interferometer, where τ is the delay-time intervals between adjacent pulses (Supplementary Information). Here I(t) represents the expectation

value of the intensity at time t. Figure 3e shows the zero delay of the normalized second-order intensity correlation function $g^2(0)$; further, three different regimes, namely, spontaneous emission (SpE), amplified spontaneous emission (ASE) and stimulated emission (StE), are evidenced. We observe the suppression of the photon bunching peak (visible in the ASE regime) in the StE regime, that is, lasing action. Furthermore, the full-width at half-maximum (FWHM) of the zero-delay $g^2(\tau)$ pulse shrinks in the SpE regime, reaches a minimum in the ASE regime and broadens in the StE regime (Fig. 3f). Such variations in the $g^2(\tau)$ pulse width are related to a nonlinear effect called the delayed threshold phenomenon or dynamical hysteresis, which occurs in a laser only when the peak intensity of a pump pulse is larger than the threshold intensity. The distinct behaviours of the $g^2(\tau)$ width in the SpE and StE regimes signify that the suppression of the photon bunching peak (Fig. 3e) at high pump intensity indeed originates from lasing instead of SpE²⁷. It is worth noting that the unity $g^2(0)$ in the SpE regime is due to the limited time resolution of the detection system (Supplementary Information).

Figure 4a,b shows the far-field interference patterns of the emission from QH ring 2 of quantum number ℓ_2 with the opposite quantum number $-\ell_2$ obtained theoretically (Fig. 4a) and experimentally (Fig. 4b). The opposite quantum number is experimentally achieved by reflecting the beam in a mirror. The interference patterns evidence fringes that are characteristic of beams carrying OAM. These fringes are observed both theoretically and experimentally, as shown in Fig. 4. QH ring 2 is designed for $|\ell_2| = 156$, and the total number of measured fringes is two times $|\ell_2|$, that is, 312. The interference patterns of the other QH rings, measured in a similar manner, confirm the successful implementation of photonic quantum Hall effect–based OAM lasers of large quantum numbers.

We reported compact and integrated QH rings capable of emitting coherent beams carrying OAM of large quantum numbers. NATURE PHYSICS LETTERS

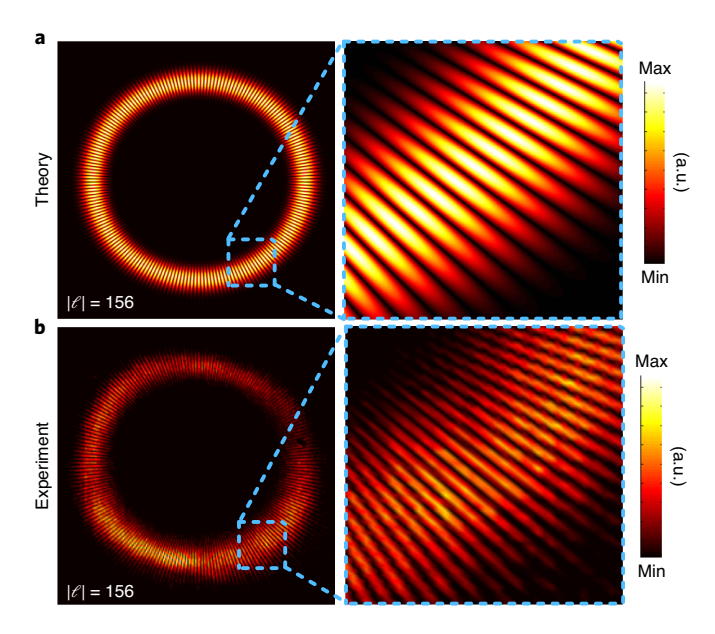


Fig. 4 | Far-field interference pattern of beams emitted from photonic QH ring lasers. a,b, Interference pattern of the emission from QH ring 2 of quantum number ℓ_2 with the opposite quantum number $-\ell_2$ obtained theoretically (**a**) and experimentally (**b**). The interference patterns evidence fringes that are characteristic of beams carrying OAM. QH ring 2 is designed for $|\ell_2| = 156$, and the total number of fringes is two times $|\ell_2|$, that is, 312. The interference patterns of QH rings 1 and 3, measured in a similar manner, exhibit the same characteristics.

The OH rings are formed by circular interfaces between topologically dissimilar photonic structures with edge states above the light cone, constituting leaky-wave circular orbits that naturally radiate orthogonal OAM. While a large separation between the quantum numbers of OAM modes decreases their crosstalk, it also constitutes a challenge that puts constraints on the type of media in which such modes can propagate. We demonstrated the coherence of the proposed QH ring lasers by measuring their second-order intensity correlation. These results demonstrate that topological nanostructures based on the quantum Hall effect can be used to uniquely generate topological light. The principle described here could be used to develop quantum light sources based on parametric processes to directly generate OAM states and increase the photon flux via multiplexing. Recent results have shown that the quantum number of certain OAM sources can be dynamically controlled^{28,29}. Similar dynamic control could be implemented using our platform. Our work opens the way to novel classical and quantum sources with applications in communication, sensing and imaging.

Online content

Any methods, additional references, Nature Research reporting summaries, source data, extended data, supplementary information, acknowledgements, peer review information; details of author contributions and competing interests; and statements of data and code availability are available at https://doi.org/10.1038/s41567-021-01165-8.

Received: 16 July 2020; Accepted: 8 January 2021; Published online: 25 February 2021

References

- Raghu, S. & Haldane, F. D. M. Analogs of quantum-Hall-effect edge states in photonic crystals. *Phys. Rev. A* 78, 033834 (2008).
- Wang, Z., Chong, Y., Joannopoulos, J. D. & Soljačić, M. Observation of unidirectional backscattering-immune topological electromagnetic states. *Nature* 461, 772–775 (2009).
- Bahari, B. et al. Nonreciprocal lasing in topological cavities of arbitrary geometries. Science 358, 636–640 (2017).
- Klembt, S. et al. Exciton-polariton topological insulator. Nature 562, 552–556 (2018).
- Khandekar, C. & Jacob, Z. Thermal spin photonics in the near-field of nonreciprocal media. New J. Phys. 21, 103030 (2019).
- Secli, M., Capone, M. & Carusotto, I. Theory of chiral edge state lasing in a two-dimensional topological system. *Phys. Rev. Res.* 1, 033148 (2019).
- Allen, L., Beijersbergen, M. W., Spreeuw, R. J. C. & Woerdman, J. P. Orbital angular momentum of light and the transformation of Laguerre-Gaussian laser modes. *Phys. Rev. A* 45, 8185 (1992).
- 8. Hall, E. H. On a new action of the magnet on electric currents. *Am. J. Math.* 2, 287–292 (1879).
- von Klitzing, K., Dorda, G. & Pepper, M. New method for high-accuracy determination of the fine-structure constant based on quantized Hall resistance. *Phys. Rev. Lett.* 45, 494–497 (1980).
- 10. Prange, R. E. & Girvin, S. M. The Quantum Hall Effect (Springer, 1987).
- Hafezi, M., Demler, E. A., Lukin, M. D. & Taylor, J. M. Robust optical delay lines with topological protection. *Nat. Phys.* 7, 907–912 (2011).
- Longhi, S. Synthetic gauge fields for light beams in optical resonators. Ont. Lett. 40, 2941–2944 (2015).
- Kruk, S. et al. Nonlinear light generation in topological nanostructures. Nat. Nanotechnol. 14, 126–130 (2019).
- Bandres, M. A. et al. Topological insulator laser: experiments. Science 359, 6381 (2018).
- Rechtsman, M. C. et al. Photonic Floquet topological insulators. Nature 496, 196–200 (2013).
- Fleury, R., Khanikaev, A. B. & Alù, A. Floquet topological insulators for sound. Nat. Commun. 7, 11744 (2016).
- Khanikaev, A. B. et al. Photonic topological insulators. Nat. Mater. 12, 233–239 (2013).
- Ma, T. & Shvets, G. All-Si valley-Hall photonic topological insulator. New J. Phys. 18, 025012 (2016).
- Shao, Z.-K. et al. A high-performance topological bulk laser based on band-inversion-induced reflection. Nat. Nanotechnol. 15, 67–72 (2019).
- Padgett, M. J. Orbital angular momentum 25 years on [invited]. Opt. Exp. 25, 11265–11274 (2017).
- Miao, P. et al. Orbital angular momentum microlaser. Science 353, 464–467 (2016).
- Carlon Zambon, N. et al. Optically controlling the emission chirality of microlasers. Nat. Photon. 13, 283–288 (2019).
- Sroor, H. et al. High-purity orbital angular momentum states from a visible metasurface laser. Nat. Photon. 14, 498–503 (2020).
- Yang, Z.-Q., Shao, Z.-K., Chen, H.-Z., Mao, X.-R. & Ma, R.-M. Spin-momentum-locked edge mode for topological vortex lasing. *Phys. Rev. Lett.* 125, 013903 (2020).
- Sarollahi, M. et al. Calculation of reflectivity spectra for semi-infinite two-dimensional photonic crystals. J. Nanophoton. 10, 046012 (2016).
- Park, H. et al. Electrically driven single-cell photonic crystal laser. Science 305, 1444–1447 (2004).
- 27. Loudon, R. *The Quantum Theory of Light* 3rd edn (Oxford Univ. Press, 2000).
- Huang, C. et al. Ultrafast control of vortex microlasers. Science 367, 1018–1021 (2020).
- Zhang, Z. et al. Tunable topological charge vortex microlaser. Science 368, 760–763 (2020).

Publisher's note Springer Nature remains neutral with regard to jurisdictional claims in published maps and institutional affiliations.

© The Author(s), under exclusive licence to Springer Nature Limited 2021

LETTERS NATURE PHYSICS

Data availability

The data that support the plots within this paper and other findings of this study are available from the corresponding author upon reasonable request.

Code availability

The computer codes that support the plots within this paper and other findings of this study are available from the corresponding author upon reasonable request.

Acknowledgements

This research was mostly supported by the Office of Naval Research Young Investigator Award (N00014-17-1-2671), the ONR JTO MRI Award (N00014-17-1-2442), the National Science Foundation Career Award (ECCS-1554021) and the Laboratory Directed Research and Development Program of Lawrence Berkeley National Laboratory under US Department of Energy contract no. DE-AC02-05CH11231. The work was partially supported by the Moore Inventor Fellows program, the DARPA DSO-NLM Program HR00111820038 and the NSF QLCI programme through grant number OMA-2016245. The work was performed in part at the San Diego Nanotechnology Infrastructure, a member of the National Nanotechnology Coordinated Infrastructure, which is supported by the National Science Foundation (ECCS-1542148). We thank M. Montero for technical assistance regarding fabrication.

Author contributions

B.K. conceived the project and guided the theoretical and experimental investigations. B.B. fabricated the samples. B.B. and L.H. performed the simulations. B.B., S.H.P., D.P., A.N. and A.E.A. performed the measurements. B.K. and Y.F. supervised the research. All the authors contributed to discussions and manuscript writing.

Competing interests

The authors declare no competing interests.

Additional information

Supplementary information The online version contains supplementary material available at https://doi.org/10.1038/s41567-021-01165-8.

Correspondence and requests for materials should be addressed to B.K.

Peer review information *Nature Physics* thanks Ren-Min Ma, Lorenzo Marrucci and the other, anonymous, reviewer(s) for their contribution to the peer review of this work.

Reprints and permissions information is available at www.nature.com/reprints.